Atmos. Meas. Tech., 5, 2859–2866, 2012
www.atmos-meas-tech.net/5/2859/2012/
doi:10.5194/amt-5-2859-2012


Atmospheric Measurement Techniques

# Using particle filter to track horizontal variations of atmospheric duct structure from radar sea clutter

**X. F. Zhao**[1,2], **S. X. Huang**[1], **and D. X. Wang**[2]

[1]College of Meteorology and Oceanography, PLA University of Science and Technology, Nanjing, China
[2]State Key Laboratory of Tropical Oceanography, South China Sea Institute of Oceanology, Chinese Academy of Sciences, Guangzhou, China

*Correspondence to:* X. F. Zhao (zxf_best@126.com)

Received: 3 April 2012 – Published in Atmos. Meas. Tech. Discuss.: 23 August 2012
Revised: 24 October 2012 – Accepted: 10 November 2012 – Published: 26 November 2012

**Abstract.** This paper addresses the problem of estimating range-varying parameters of the height-dependent refractivity over the sea surface from radar sea clutter. In the forward simulation, the split-step Fourier parabolic equation (PE) is used to compute the radar clutter power in the complex refractive environments. Making use of the inherent Markovian structure of the split-step Fourier PE solution, the refractivity from clutter (RFC) problem is formulated within a nonlinear recursive Bayesian state estimation framework. Particle filter (PF), which is a technique for implementing a recursive Bayesian filter by Monte Carlo simulations, is used to track range-varying characteristics of the refractivity profiles. Basic ideas of employing PF to solve RFC problem are introduced. Both simulation and real data results are presented to confirm the feasibility of PF-RFC performances.

## 1 Introduction

The refractive environment is generally characterized by the refractivity profile (N-profile) or the modified refractivity profile (M-profile), and there are many techniques that measure or predict the tropospheric index of refraction. Conventional methods of the refractive index measurement consisting of detecting height dependence of temperature, pressure and humidity performed by radiosondes, microwave refractometers, or rocketsondes have some drawbacks, such as expensive and/or difficult deployment. Moreover, these measurements tend to provide estimations of refractivity versus height only at a single range (Halvey, 1983; Weckwerth et al., 2005; Yan et al., 2006; Yu et al., 2009; Cheng et al., 2012). Therefore, it is necessary to develop more sophisticated methods for refractivity detection.

Richter (1969) has pointed out that the temporal and spatial variations of radar echoes are related to the temporal and spatial variations in the layers of the refractivity profile, which motivates the research of atmospheric refractivity estimation from radar clutter returns, i.e. refractivity from clutter (RFC). More investigations concerning the phenomenology of sea clutter returns from extended ranges associated with ducting conditions have been discussed in the work of Gossard and Strauch (1983). The idea of RFC is to extract the refractive information contained in the sea surface clutter, as well as ground echoes (Park and Fabry, 2011). The advantages of RFC are that it can provide a synoptic characterization of the duct over the spatial extent of the radar and it overcomes the necessity of additional hardware or extra meteorological/electromagnetic measurements (Vasudevan et al., 2007). In addition, the results of RFC can be used to estimate moisture fields with high temporal and spatial resolution with application in understanding thunderstorm initiation (Weckwerth et al., 2005).

RFC is a complex inverse problem because the relationship between refractivity parameters and radar sea clutter is clearly nonlinear and ill-posed. It is difficult to get analytical solutions according to current theories, and global optimization method might be a good choice to get approximate solutions (Wang et al., 2009). In the last decade, many advances have been made in remotely sensing refractivity parameters from radar sea clutter. In order to simplify the computation, most of these works treat the refractive environment horizontally homogeneous (Rogers et al., 2000; Barrios, 2004; Kraut

et al., 2004; Yardim et al., 2006, 2009; Douvenot et al., 2008; Huang et al., 2009; Wang et al., 2009; Zhao et al., 2011; Zhao and Huang, 2011, 2012). Although the spatial change of tropospheric refractivity is larger with height than with range and generally the horizontal homogeneity assumptions of the refractive environments are demonstrated to be reasonable (Hitney et al., 1985; Goldhirsh and Dockery, 1998), the environment can change drastically at air/mass boundaries associated with wave clones and land/ocean interfaces (Barrios, 1992). Therefore, some studies for range-varying estimations have also been investigated.

Gerstoft et al. (2003a, b) proposed the usage of the genetic algorithm (GA) to perform global refractivity estimation. In their work, the authors presented a method to model both the range- and the height-dependent refractive environment using a total of 11 parameters (5 parameters describe vertical structure and 6 parameters describe horizontal variations). Although GA does well in estimating the maximum a posteriori (MAP) solution, it gives poor results in calculating the multi-dimensional integrals required to obtain means, variances and underlying probability distribution functions of the estimated parameters. Accurate distributions can be obtained using MCMC (Markov chain Monte Carlo) samplers, such as the Metropolis-Hastings and Gibbs sampling algorithms (Yardim et al., 2007). The drawback of MCMC is that it requires a large number of samples and becomes impractical with increasing number of unknowns. Vasudevan et al. (2007) exploited the inherent Markovian structure of the split-step Fourier PE solution and showed how recursive Bayesian estimation when combined with forward and Viterbi algorithms can be used to solve the problem of estimating RFC in a sequential manner. Through establishing many pre-computed, modeled radar clutter returns for different environments in a database, Douvenot et al. (2010) inverted real-time profiles based on finding the optimal environment from the database.

Recent developments have demonstrated that particle filter (PF) is an emerging and powerful methodology for sequential signal processing with a wide range of applications in science and engineering (Arulampalam et al., 2002; Lee and Chia, 2002; Djuric et al., 2003; Hlinomaz and Hong, 2009). Based on the concept of sequential importance sampling and the use of Bayesian theory, PF is particularly useful in dealing with nonlinear and non-Gaussian problems. The underlying principle of the methodology is the approximation of relevant distributions with random measures composed of particles and their associated weights. Yardim et al. (2008) have used PF to track temporal and spatial change of refractivity profile from radar sea clutter, mainly for range-independent case. In their work, the observations were assumed to be collected at different time point, each time they could obtain an integral observed data. Different from Yardim's work, in this paper, PF is extended to range-varying refractivity estimations from just radar observations. The reminder of this paper is organized as follows. In Sect. 2, the state-space model including state evolution equation and observation equation is introduced. The fundamentals of PF-RFC algorithm are described in Sect. 3. Section 4 shows the performances of PF-RFC estimations, including idea duct model simulations and real data results.

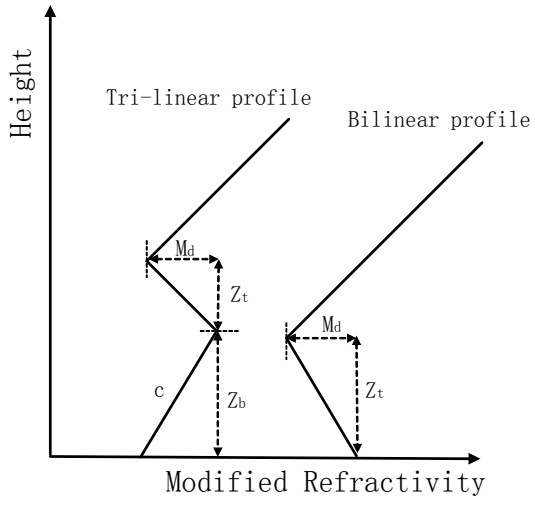


**Fig. 1.** The sketch map of trilinear profile and bilinear profile.

## 2 State-space model

### 2.1 Atmospheric duct model

In the marine environment, there exist three types of atmospheric ducts: the evaporation duct, surface-based duct, and elevated duct. For the purposes of propagation studies, several parameterized duct models are used to present the height-dependent duct structures, in which trilinear profile (see Fig. 1) is quite versatile in its ability to include refractivity representations of the commonly atmospheric ducts (Rogers, 1996).

As described in Fig. 1, trilinear profile can be represented by four parameters, i.e. base height $z_b$, thickness $z_t$, M-deficit $M_d$, and slope of refractivity in the lower layer $c$. The modified refractivity $M$ for the trilinear profile can be determined at any height $z$ by the relationship:

$$M(z) = M_0 + \begin{cases} cz, & \text{for } z \le z_b \\ cz_b - \frac{M_d}{z_t}(z - z_b), & \text{for } z_b < z \le z_b + z_t \\ cz_b - M_d + 0.118(z - z_b - z_t), & \text{for } z > z_b + z_t \end{cases} \quad (1)$$

where $M_0$ is the modified refractivity at the sea surface usually taken as 330 M-units. When the value of base height reduces to zero, trilinear profile will end up with a bilinear profile, which means that the bottom of the duct touches the ground.

Let $\boldsymbol{x}$ be the state vector of refractivity parameters. Then, for trilinear profile model, $\boldsymbol{x} = [z_b, z_t, M_d, c]^T$. Since the index of refraction is a function of physical quantities such as

pressure, temperature and humidity, it is reasonably assumed that the parameters of the refractivity do not undergo drastic changes over small range intervals. Moreover, the correlation of the refractive process suggests characterizing the relationship between the parameters from one range step to another by a Markov process (Vasudevan et al., 2007). Thus, the evolution of the refractivity parameters over range can be expressed as

$$\boldsymbol{x}_{k+1} = \Gamma(\boldsymbol{x}_k) + \boldsymbol{w}_k \tag{2}$$

where $\Gamma(\cdot)$ is the system transition function and $\boldsymbol{w}_k$ models the uncertainty in the variations of refractivity parameters over range. Generally, it is assumed to be a zero mean, white Gaussian sequence with covariance matrix $\mathbf{Q}_k$, and is independent of past and current states.

### 2.2 Measurement equation

Before performing RFC estimations, a forward simulation of the received radar sea clutter power $P_c$ has to be computed. In the absence of receiver noise, the received signal power from the clutter can be modeled as a function of the one-way propagation loss $L_{\text{loss}}$ in decibels (Gerstoft et al., 2003a):

$$P_c(r_k, \boldsymbol{x}_k) = -2L_{\text{loss}}(r_k, z_0, \boldsymbol{x}_k) + 10\log_{10}(r_k) + C, \tag{3}$$

where $r_k$ is the propagation range, $z_0$ is the height of sea surface level, $\boldsymbol{x}_k$ is the refractivity parameter vector at range $r_k$, and $C$ is a constant that includes wavelength, radar cross-section (RCS), transmitter power, antenna gain, etc. In Eq. (3), propagation loss $L_{\text{loss}}$ can be computed as (Barrios, 1991)

$$L_{\text{loss}}(r_k, z) = -10\log_{10}\left(\frac{\lambda^2 |u(r_k, z)|^2}{(4\pi)^2 r_k}\right) \tag{4}$$

where $\lambda$ is the wavelength, and $u$ is the electric field that can be computed numerically using the split-step Fourier PE method (Kuttler and Dockery, 1991; Barrios, 1992):

$$u(r_{k+1}, z) = \exp\left[ik_0 \delta r M(r_k, z) 10^{-6}\right] F^{-1}\left\{\exp\left[i\frac{p^2 \delta r}{2k_0}\right] F\{u(r_k, z)\}\right\} \tag{5}$$

where $k_0$ is the free space wave number, $\delta r$ is the range increment, defined by $\delta r = r_{k+1} - r_k$. $M(r_k, z)$ is the modified refractivity at range $r_k$ and height $z$, which can be determined by the state vector $\boldsymbol{x}_k$ (see Eq. (1)). $F\{\cdot\}$ and $F^{-1}\{\cdot\}$, respectively, are the Fourier transform and inverse Fourier transform operator, and $p$ is the Fourier transform variable. Detailed description of the split-step Fourier PE solution has been given in the works completed by Kuttler and Dockery (1991).

From Eq. (5), it is clear that if the electric field at range $r_k$ is known, the field at the next range $r_{k+1}$ is only determined by the state vector $\boldsymbol{x}_k$, which formulates a Markovian structure. If the initial field $u(r_0, z)$ at the transmitter range $r_0 = 0$ is known, recurring to the recursive relationship given in Eq. (5), the field at range $r_{k+1}$ is a function of all the refractivity parameters up to range $r_{k+1}$. Thus, we must begin with an initial field $u(r_0, z)$ in order to propagate the field forward. Initial field is a function of radar system parameters. For a detailed computation, refer to Barrios (1991).

Let $\boldsymbol{y}$ be the measurement vector, $H(\cdot)$ be the measurement function, and $\boldsymbol{v}$ be the measurement noise. Then, the noisy measurements related to the state vector can be expressed as

$$\boldsymbol{y}_k = H(\boldsymbol{x}_k) + \boldsymbol{v}_k \tag{6}$$

where the measurement function $H(\cdot)$ is determined by Eqs. (3)–(5). $\boldsymbol{v}_k$ is another zero mean, white Gaussian sequence with covariance matrix $\mathbf{R}_k$, and it is independent of past and present states and the process noise.

## 3 Particle filter

According to Eqs. (2) and (6), the RFC problem has been modeled as a nonlinear continuous state-space estimation problem:

$$\begin{cases} \boldsymbol{x}_k = \Gamma(\boldsymbol{x}_{k-1}) + \boldsymbol{w}_{k-1} \\ \boldsymbol{y}_k = H(\boldsymbol{x}_k) + \boldsymbol{v}_k \end{cases} \tag{7}$$

The objective now is to estimate the state vector $\boldsymbol{x}_k$ from the measurement vector $\boldsymbol{y}_k$.

The method that has been investigated most and that has been frequently applied in practice to the state-space estimation is the Kalman filter (KF) (Anderson and Moore, 1979). KF is optimal in the important case when the equations are linear and the noises are independent and Gaussian. In this situation, the distributions of interest (filtering, predictive, or smoothing) are also Gaussian and the KF can compute them exactly without approximations. For scenarios where the models are nonlinear or the noise is non-Gaussian, various approximate methods have been proposed of which the extended Kalman filter (EKF) is perhaps the most prominent of all. EKF is based on linearizing the state and/or measurement equations using Taylor's series expansions. In RFC estimation, using EKF is problematic because the refractivity parameters of interest appear in the complex exponential in Eq. (5) which when linearized leads to instability of EKF and very poor estimates of refractivity parameters (Sheng, 2011).

Recently, particle filter (PF) method has become an important alternative to EKF. With PF, continuous distributions are approximated by discrete random measures, which are composed of weighted particles, where the particles are samples of the unknown states from the state space, and the particle weights are probability masses computed by Bayes' theory. The advantage of PF over other filtering methods is in that the exploited approximation does not involve linearization around current estimates but rather approximations in

the representation of the desired distributions by discrete random measures (Djuric et al., 2003). There are many different variants of PF such as sequential importance resampling particle filter (SIRPF), regularized particle filter (RPF), Gaussian particle filter (GPF), and auxiliary particle filter (APF). The SIRPF is used throughout this work.

In order to develop the details of the algorithm, let $\left\{\boldsymbol{x}_{0:k}^i, w_k^i\right\}_{i=1}^{N_\mathrm{p}}$ denote a cloud of $N_\mathrm{p}$ particles to approximate the estimate of the posterior probability density function (PDF) $p(\boldsymbol{x}_{0:k}|\boldsymbol{y}_{1:k})$, where $\left\{\boldsymbol{x}_{0:k}^i, i=0,\cdots,N_\mathrm{p}\right\}$ is a set of support points with associated weights $\left\{w_k^i, i=0,\cdots,N_\mathrm{p}\right\}$ and $\boldsymbol{x}_{0:k}=\left\{\boldsymbol{x}_j, j=0,\cdots,k\right\}$ is the set of all states up to time $k$. The weights are normalized such that $\sum_i w_k^i=1$. Then, the posterior PDF at time $k$ can be approximated as

$$p(\boldsymbol{x}_{0:k}|\boldsymbol{y}_{1:k}) \approx \sum_{i=1}^{N_\mathrm{p}} w_k^i \delta(\boldsymbol{x}_{0:k}-\boldsymbol{x}_{0:k}^i). \tag{8}$$

One therefore has a discrete weighted approximation to the true posterior PDF. The weights are chosen using the principle of importance sampling (Doucet, 1998). This principle relies on the following.

Sometimes, it is difficult or impossible to directly sample from the posterior PDF $p(\boldsymbol{x}_{0:k}|\boldsymbol{y}_{1:k})$. Then, a new density $\pi(\boldsymbol{x})$ that can be evaluated and that is chosen to satisfy $p(\boldsymbol{x})\propto\pi(\boldsymbol{x})$ is defined. Additionally, let $\boldsymbol{x}^i\sim q(\boldsymbol{x}),\ i=1,\cdots,N_\mathrm{p}$ be samples that are easily generated from a proposal $q(\cdot)$, which is referred to as the importance density.

The weights of each normalized particle are then defined as

$$w_k^i \propto \frac{\pi(\boldsymbol{x}^i)}{q(\boldsymbol{x}^i)}. \tag{9}$$

Since $p(\boldsymbol{x})\propto\pi(\boldsymbol{x})$, the normalized particle weights can also be obtained via

$$w_k^i \propto \frac{p(\boldsymbol{x}_{0:k}^i|\boldsymbol{y}_{1:k})}{q(\boldsymbol{x}_{0:k}^i|\boldsymbol{y}_{1:k})}. \tag{10}$$

The importance density is chosen to factorize such that

$$q(\boldsymbol{x}_{0:k}|\boldsymbol{y}_{1:k}) = q(\boldsymbol{x}_k|\boldsymbol{x}_{0:k-1},\boldsymbol{y}_{1:k})q(\boldsymbol{x}_{0:k-1}|\boldsymbol{y}_{1:k-1}). \tag{11}$$

Then, one can obtain samples $\boldsymbol{x}_{0:k}^i\sim q(\boldsymbol{x}_{0:k}|\boldsymbol{y}_{1:k})$ by augmenting each of the existing samples $\boldsymbol{x}_{0:k-1}^i\sim q(\boldsymbol{x}_{0:k-1}|\boldsymbol{y}_{1:k-1})$ with the new state $\boldsymbol{x}_k^i\sim q(\boldsymbol{x}_k|\boldsymbol{x}_{0:k-1},\boldsymbol{y}_{1:k})$. To derive the weight update equation, $p(\boldsymbol{x}_{0:k}|\boldsymbol{y}_{1:k})$ is expressed as

$$\begin{aligned} p(\boldsymbol{x}_{0:k}|\boldsymbol{y}_{1:k}) &= \tfrac{p(\boldsymbol{y}_k|\boldsymbol{x}_k)p(\boldsymbol{x}_k|\boldsymbol{x}_{k-1})}{p(\boldsymbol{y}_k|\boldsymbol{y}_{1:k-1})}p(\boldsymbol{x}_{0:k-1}|\boldsymbol{y}_{1:k-1}) \\ &\propto p(\boldsymbol{y}_k|\boldsymbol{x}_k)p(\boldsymbol{x}_k|\boldsymbol{x}_{k-1})p(\boldsymbol{x}_{0:k-1}|\boldsymbol{y}_{1:k-1}) \end{aligned} \tag{12}$$

By substituting Eqs. (11) and (12) into Eq. (10), the weight update equation can then be shown to be

$$\begin{aligned} w_k^i &\propto \frac{p(\boldsymbol{y}_k|\boldsymbol{x}_k^i)p(\boldsymbol{x}_k^i|\boldsymbol{x}_{k-1}^i)p(\boldsymbol{x}_{0:k-1}^i|\boldsymbol{y}_{1:k-1})}{q(\boldsymbol{x}_k^i|\boldsymbol{x}_{0:k-1}^i,\boldsymbol{y}_{1:k})q(\boldsymbol{x}_{0:k-1}^i|\boldsymbol{y}_{1:k-1})} \\ &= w_{k-1}^i\frac{p(\boldsymbol{y}_k|\boldsymbol{x}_k^i)p(\boldsymbol{x}_k^i|\boldsymbol{x}_{k-1}^i)}{q(\boldsymbol{x}_k^i|\boldsymbol{x}_{0:k-1}^i,\boldsymbol{y}_{1:k\cdot})} \end{aligned} \tag{13}$$

If the importance density describes a Markovian process, then the importance density becomes only dependent on the previous state $\boldsymbol{x}_{k-1}$ and the current measurement $\boldsymbol{y}_k$. In this case, Eq. (13) can be expressed as

$$w_k^i \propto w_{k-1}^i\frac{p(\boldsymbol{y}_k|\boldsymbol{x}_k^i)p(\boldsymbol{x}_k^i|\boldsymbol{x}_{k-1}^i)}{q(\boldsymbol{x}_k^i|\boldsymbol{x}_{k-1}^i,\boldsymbol{y}_k)}. \tag{14}$$

A key issue in PF is choosing an appropriate importance density. Generally, it is often convenient to choose the importance density to be the prior state density $p(\boldsymbol{x}_k^i|\boldsymbol{x}_{k-1}^i)$. This handling way is adopted in SIRPF. When the prior is used, the weight update equation can be expressed as

$$w_k^i \propto w_{k-1}^i p(\boldsymbol{y}_k|\boldsymbol{x}_k^i). \tag{15}$$

The SIRPF resamples the particles with replacement at every time increment and sets the resampled particle weight to $1/N_\mathrm{p}$. Then, Eq. (15) can be reduced to be

$$w_k^i \propto p(\boldsymbol{y}_k|\boldsymbol{x}_k^i). \tag{16}$$

This removes the dependency of the current particle weight to the previous particle weight. The weights given by the proportionality in Eq. (16) should be normalized before the resampling stage. The stratified sampling scheme (Carpenter et al., 1999) is adopted in this paper. Since the particle weights are now equal, after resampling the state estimate is

$$\hat{\boldsymbol{x}}_{k|k} = \frac{1}{N_\mathrm{p}}\sum_{i=1}^{N_\mathrm{p}}\boldsymbol{x}_{k|k}^i. \tag{17}$$

The SIRPF is popular because it is easy to implement. Consequently it has been used in numerous non-linear/non-Gaussian filtering applications. A significant drawback of the SIRPF is that it does not incorporate current measurements into the importance density. Thus, it may require a large number of particles in order to work well if the prior density and likelihood function have only a small region of overlap. Additional detailed discussions on SIRPF can be found in the tutorials provided in Doucet (1998) and Arulampalam et al. (2005).

The application of the SIRPF to RFC estimations can be summarized as follows:

*Initialization:* It is assumed that the initial PDF $p(\boldsymbol{x}_0|\boldsymbol{y}_0)\equiv p(\boldsymbol{x}_0)$ of the state vector is available. Start from a cloud of $N_\mathrm{p}$ random samples $\left\{\boldsymbol{x}_0^i, 1/N_\mathrm{p}\right\}_{i=1}^{N_\mathrm{p}}$ with equal weight from $p(\boldsymbol{x}_0)$. In RFC estimations, historical observations and/or possibly an in situ measurement of refractivity profile at the radar can be used to form a prior distribution on $\boldsymbol{x}_0$.

*Prediction:* Each sample is passed through the state equation, i.e. Eq. (2), to obtain the samples from the prior at time step $k$: $\tilde{\boldsymbol{x}}_k^i=\Gamma(\boldsymbol{x}_{k-1}^i)+\boldsymbol{w}_{k-1}^i$.

*Update:* On receipt of the measurement $\boldsymbol{y}_k$, evaluate the likelihood function of each prior sample by the measurement equation: $p(\boldsymbol{y}_k|\tilde{\boldsymbol{x}}_k^i) = H(\tilde{\boldsymbol{x}}_k^i) + \boldsymbol{v}_k^i$. Then, compute the normalized weight for each sample:

$$w_k^i = \frac{p(\boldsymbol{y}_k|\tilde{\boldsymbol{x}}_k^i)}{\sum_{j=1}^{N_\mathrm{p}} p(\boldsymbol{y}_k|\tilde{\boldsymbol{x}}_k^j)} \tag{18}$$

$$p(\boldsymbol{y}_k|\tilde{\boldsymbol{x}}_k^i) \propto \exp\left\{-\frac{1}{2}\left[\boldsymbol{y}_k - H(\tilde{\boldsymbol{x}}_k^i)\right]^T \mathbf{R}_k^{-1}\left[\boldsymbol{y}_k - H(\tilde{\boldsymbol{x}}_k^i)\right]\right\} \tag{19}$$

Thus, define a discrete distribution over $\left\{\tilde{\boldsymbol{x}}_k^i, \boldsymbol{w}_k^i\right\}_{i=1}^{N_\mathrm{p}}$. Now resample $N_\mathrm{p}$ times from the discrete distribution to generate samples $\left\{\boldsymbol{x}_k^i, 1/N_\mathrm{p}\right\}_{i=1}^{N_\mathrm{p}}$.

## 4 PF-RFC results

In this section, the performances of PF-RFC estimations are tested. First, a horizontal varying refractive environment is simulated by the idea trilinear duct model and the corresponding synthetic propagation losses at sea level are used to quantify the performance of PF-RFC estimations. Then, a set of real refractivity and radar sea clutter data collected in Wallops98 experiments are used.

### 4.1 Simulation results

In our simulations, the Space and Range Radar (SPANDAR) parameters operated in Wallops98 experiments are used, i.e. a vertical polarization antenna with operational frequency of 2.84 GHz, horizontal beamwidth of 0.39 deg, elevation angle of 0 deg, range bin width of 600 m, and antenna height of 30.78 m (see Gerstoft et al., 2003a).

Figure 2 compares the propagation losses with respect to the distance at sea level obtained from three different surface-based duct profiles, where the duct heights for two similar profiles are near 150 m and the other one is 50 m. From Fig. 2, it can be seen that different refractivity profiles correspond to different propagation loss distributions, and the propagation losses of the lower duct are significantly different from those of the other two higher ducts. This phenomenon indicates that the refractive information can be reflected by the energy distribution, which makes the idea of RFC possible. When the refractivity profiles are similar, the differences between their propagation loss are small, but increase with the distance. However, the structures, especially within 10 km near the transmitter, are very close.

In practical operations, the range bin width for measurements is usually several hundred meters. If the propagation loss at each range step is used as an independent observation, this may result in deficiencies in the observations and bring about larger errors in RFC estimations. In our computations, the range step $\delta r$ for the split-step Fourier PE solution

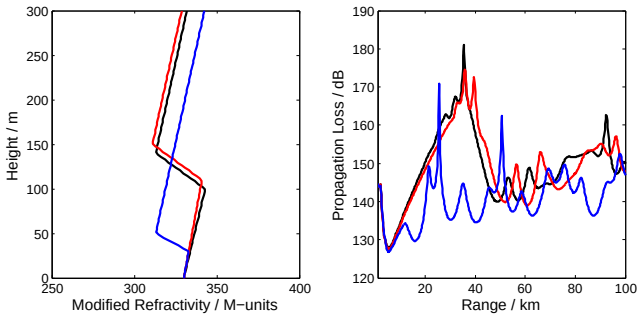


**Fig. 2.** Three different surface-based duct profiles and their corresponding propagation losses versus distance at the sea level.

is set to be 600 m, while the state evolution range is set to be 6 km. The refractive environment between the two state profiles is obtained using linear interpolation. Thus, we could get 10 discrete point observations in every state evolution. The propagation range in this paper is selected to be 60 km.

Here, we consider the following state evolution equations as a simulated example.

$$\begin{cases} z_{\mathrm{b},k+1} = z_{\mathrm{b},k} + 0.1 \times k^2/(k+1) \\ z_{\mathrm{t},k+1} = z_{\mathrm{t},k} + 0.1 \times k \\ M_{\mathrm{d},k+1} = M_{\mathrm{d},k} + 0.1 \times k \\ c_{k+1} = c_k - 0.0004 \times k^{1.2} \end{cases} \tag{20}$$

The initial state is taken to be $\boldsymbol{x}_0 = [100\,\mathrm{m},\ 40\,\mathrm{m},\ 30\,\text{M-units},\ 0.13\,\text{M-units}\,\mathrm{m}^{-1}]^T$; the covariance for the process noise $\mathbf{Q}_k$ and measurement noise $\mathbf{R}_k$ are respectively set to be $\mathbf{Q}_k = \mathrm{diag}\left\{\left[(10\,\mathrm{m})^2, (10\,\mathrm{m})^2, (10\,\text{M-units})^2, \left(0.1\,\text{M-units}\,\mathrm{m}^{-1}\right)^2\right]\right\}$ and $\mathbf{R}_k = \mathrm{diag}\left\{(3\,\mathrm{dB})^2\right\}$. The prior distributions of each parameter are randomly generated from a given parameter bounds. The range of base height is $50 \sim 150$ m, thickness $5 \sim 80$ m, M-deficit $5 \sim 60$ M-units, and slope $0.1 \sim 0.2$ m M-units$^{-1}$.

In order to quantify PF-RFC performance, the root-mean-square error (RMSE) is used:

$$\mathrm{RMSE}(\hat{\boldsymbol{x}}) = \left[\frac{1}{N_\mathrm{s} \times N_\mathrm{MC}} \sum_{i=1}^{N_\mathrm{MC}} \sum_{k=1}^{N_\mathrm{S}} (\hat{\boldsymbol{x}}_k - \boldsymbol{x}_k)^2\right]^{1/2}, \tag{21}$$

where $N_\mathrm{MC}$ is the number of Monte Carlo (MC) runs, and $N_\mathrm{S}$ is the number of state evolutions.

As mentioned above, the importance density of SIRPF does not incorporate current measurements. Thus, the performance of SIRPF may be sensitive to the number of particles. Table 1 shows the RMSE values for different particles averaged over 10 MC runs.

The results given in Table 1 indicate that PF-RFC algorithm can successfully track range-varying refractivity profiles. The RMSE values are downtrending with the increment of particle number. With more particles, however, it requires much more computation time. Taking estimation accuracy

**Table 1.** RMSE values for different particles averaged over 10 MC runs.

| *Particle number* | $z_b$ (m) | $z_t$ (m) | $M_d$ (M-units) | $c$ (M-units m$^{-1}$) |
|---|---|---|---|---|
| 100 | 2.6602 | 2.4770 | 2.4192 | 0.0227 |
| 200 | 0.9746 | 1.6886 | 1.9926 | 0.0182 |
| 300 | 1.0915 | 1.0893 | 1.6205 | 0.0171 |
| 400 | 1.0648 | 1.1412 | 1.5716 | 0.0137 |
| 500 | 0.7899 | 1.0547 | 1.1295 | 0.0164 |
| 800 | 0.6895 | 0.7276 | 0.9357 | 0.0098 |
| 1000 | 0.6566 | 0.4924 | 0.7402 | 0.0105 |
| 2000 | 0.7457 | 0.4848 | 0.3629 | 0.0094 |

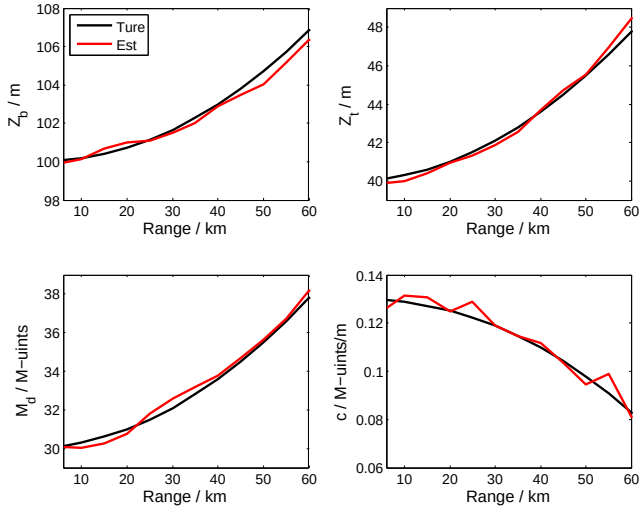


**Fig. 3.** Typical results for PF-RFC estimations of 800 particles.

and efficiency into consideration, 800 particles are used in the following computation. A typical result for the 800 particles scenario described above is shown in Fig. 3.

### 4.2 Real data results

To test PF-RFC estimations with real data, the radar sea clutter measurement collected in Wallops98 is used. The corresponding refractivity profiles are measured by a helicopter-borne instrument flying to and from 150° radial from the shore to a distance of approximately 60 km out to sea. The clutter return (dB) observed by the radar along azimuth 150° and the contour plot of the corresponding modified refractivity versus range and height are shown in Fig. 4. Detailed information about Wallops98 experiments can be found in the works completed by Rogers et al. (2000) and Gerstoft et al. (2003a, b).

From the bottom plot of Fig. 4, the contour shows a little range variability of the refractive environment. Within 6 km range bin, however, the horizontal change of the refractivity is not very strong. Thus, in real data estimations,

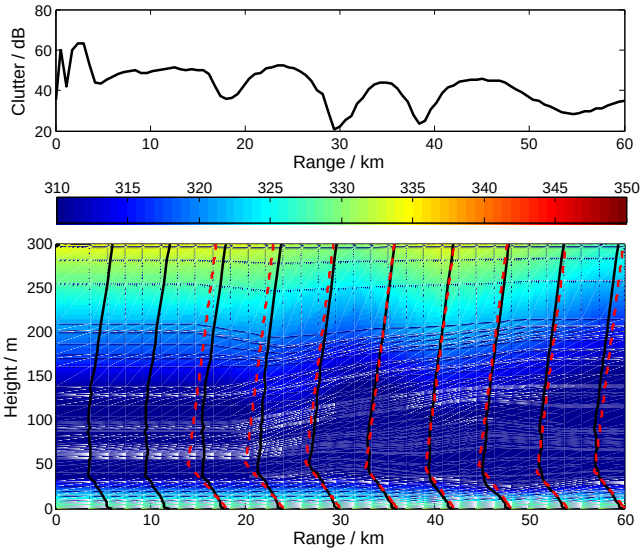


**Fig. 4.** The clutter return (dB) observed by the radar along azimuth 150° (top), and the contour plot of the corresponding modified refractivity versus range and height (bottom). The black lines indicate the measured profiles at every 6-km range bin, and the red dashed lines indicate the estimated profiles.

the range-varying characteristics of the refractivity within 6 km range bin are assumed to be a Gaussian random process. Owing to the duct, structures in Fig. 4 (black lines) are approximate to bilinear profiles which could be modeled by two parameters, i.e. thickness and M-deficit. Here the covariance for the process noise $\mathbf{Q}_k$ and measurement noise $\mathbf{R}_k$ are respectively set to be $\mathbf{Q}_k = \mathrm{diag}\left\{\left[(10\,\mathrm{m})^2, (10\,\text{M-units})^2\right]\right\}$ and $\mathbf{R}_k = \mathrm{diag}\left\{(3\,\mathrm{dB})^2\right\}$. The prior distributions of thickness are randomly generated from 5 m to 80 m, and M-deficit from 5 M-units to 60 M-units.

Using PE to simulate the electric field propagations in the troposphere does not obtain correct results for very short ranges (Gerstoft et al., 2003a). Thus in our retrievals, the first 10 km clutter data are not used. The atmosphere between 0 and 18 km is assumed to be horizontally homogeneous, which is estimated only by clutter data between 10 and 18 km.

The refractivity profiles estimated using real clutter data are also shown in the bottom plot of Fig. 4 (read dashed line). Compareing retrievals with the measured profiles, it can be seen that the features of the range-varying nature of the duct are captured, but the first two retrievals are not very good. This phenomenon can be ascribed to prior distributions of the state vector and/or the measurement errors of the used observation data. However, the final goal of the refractivity estimation is not to give the exact refractivity profiles, but to propose potential structures that could be able to render an approximation of the real atmospheric condition to predict microwave propagation for

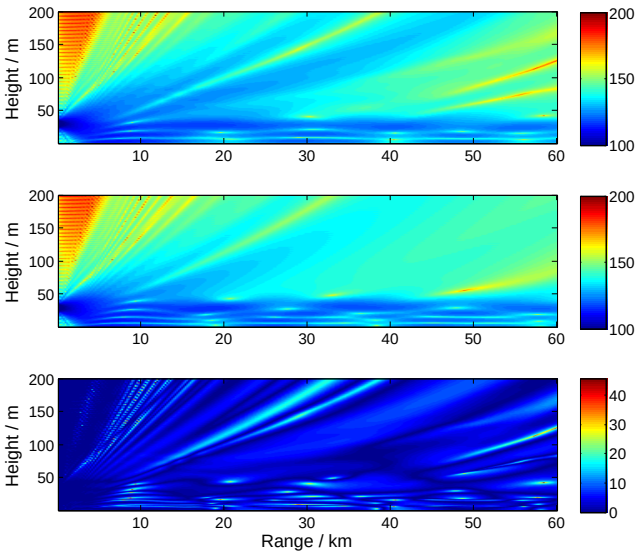


**Fig. 5.** Coverage diagrams (dB) of propagation loss corresponding to the helicopter profiles (top), estimated profiles (middle), and the absolute difference between the above two diagrams (bottom).

assessing the performance of both communications and radar systems (Douvenot et al., 2008).

Figure 5 shows the coverage diagrams (dB) of the modeled propagation loss computed by the split-step PE method using the measured refractivity and the estimated profiles. The top diagram shows the propagation loss corresponding to the helicopter profiles, and the middle diagram corresponding to the estimated profiles. It is obviously seen that, owing to the existence of the surface-based ducts, the radar signal is remarkably trapped in the duct, which increases the maximum radar channel range. The absolute difference of the above two diagrams is displayed at the bottom. Most of the differences are controlled within 20 dB, which demonstrates how well the estimated profiles are able to predict the propagation characteristics.

## 5 Conclusions

RFC is a novel technique that plays an important role in the full usage of radar systems. This paper has shown how PF can be coupled with the split-step Fourier PE solution to track range-varying refractive environments from radar sea clutter. The performances of PF-RFC algorithm are tested by both simulations and real data estimations. Through computing RMSE of the retrievals, the simulation results of different particles are analyzed. Taking estimation accuracy and efficiency into account, 800 particles are used in the real data computations. Although the results show promise, further work is required to evaluate the performance of the method with more real clutter data.

*Acknowledgements.* This work is supported by the National Natural Science Foundation of China (Grant No. 41175025) and the Major State Basic Research Development Program of China (Grant No. 2011CB403504). The real data used in our computations are acquired from SAGA which is an inversion software package completed by Gerstoft P. SAGA and is available from: http://www.mpl.ucsd.edu/people/gerstoft/saga.

Edited by: P. H. Xie

## References

Anderson, B. D. and Moore, J. B.: Optimal Filtering, Englewood Cliffs, New Jersey, Prentice-Hall, 1979.

Arulampalam, M. S., Maskell, S., Gordon, N., and Clapp, T.: A tutorial on particle filters for online nonlinear/non-Gaussian Bayesian tracking, IEEE Trans. Signal Process., 50, 174–188, 2002.

Barrios, A. E.: Radio wave propagation in horizontally inhomogeneous environments by using the parabolic equation method, Technical Report 1430, San Diego, California, 1991.

Barrios, A. E.: Parabolic equation modeling in horizontally inhomogeneous environments, IEEE Trans. Antennas Propag., 40, 791–797, 1992.

Barrios, A. E.: Estimation of surface-based duct parameters from surface clutter using a ray trace approach, Radio Sci., 39, RS6013, doi:10.1029/2003RS002930, 2004.

Carpenter, J., Clifford, P., and Fearnhead, P.: Improved particle filter for nonlinear problems, IEE Proc. – Radar, Sonar Navig., 146, 2–7, 1999.

Cheng, Y. H., Zhao, Z. W., and Zhang, Y. S.: Statistical analysis of the lower atmospheric ducts during monsoon period over the South China Sea, Chin. J. Radio Sci., 27, 268–274, 2012.

Djuric, P. M., Kotecha, J. H., Zhang, J., Huang, R., Ghirmai, T., Bugallo, M. F., and Miguez, J.: Particle Filtering. IEEE Signal Proc. Mag., 20, 19–38, 2003.

Doucet, A.: On sequential Monte Carlo methods for Bayesian filtering, Dept. Eng., Univ. Cambridge, UK, Tech. Rep., 1998.

Douvenot, R., Fabbro, V., Gerstoft, P., Bourlier, C., and Saillard, J.: A duct mapping method using least squares support vector machines, Radio Sci., 43, RS6005, doi:10.1029/2008RS003842, 2008.

Douvenot, R., Fabbro, V., Gerstoft, P., Bourlier, C., and Saillard, J.: Real time refractivity from clutter using a best fit approach improved with physical information, Radio Sci., 45, RS1007, doi:10.1029/2009RS004137, 2010.

Gerstoft, P., Rogers, L. T., Krolik, J. L., and Hodgkiss, W. S.: Inversion for refractivity parameters from radar sea clutter, Radio Sci., 38, 8053, doi:10.1029/2002RS002640, 2003a.

Gerstoft, P., Rogers, L. T., Hodgkiss, W. S., and Wagner, L. J.: Refractivity estimation using multiple elevation angles, IEEE J. Oceanic Eng., 28, 513–525, 2003b.

Goldhirsh, J. and Dockery, D.: Propagation factor errors due to the assumption of lateral homogeneity, Radio Sci., 33, 239–249, 1998.

Gossard, E. E. and Strauch, R. G.: Radar Observation of Clear Air and Clouds, Elsevier, New York, 1983.

Halvey, R. A.: Radiosonde errors and spurious surface based ducts, Proc. IEEE, Part F, 130, 643–648, 1983.

Hitney, H. V., Richter, J. H., Pappert, R. A., Anderson, K. D., and Baumgartner, G. B.: Tropospheric radio propagation assessment. Proc. IEEE, 73, 265–283, 1985.

Hlinomaz, P. and Hong, L.: A multi-rate multiple model track-before-detect particle filter, Math. Comput. Model., 49, 146–162, 2009.

Huang, S. X., Zhao, X. F., and Sheng, Z.: Refractivity estimation from radar sea clutter, Chin. Phys. B, 18, 5091–5097, 2009.

Kraut, S., Anderson, R. H., and Krolik, J. L.: A generalized Karhunen-Loeve basis for efficient estimation of tropospheric refractivity using radar clutter, IEEE Trans. Signal Process., 52, 48–60, 2004.

Kuttler, J. R. and Dockery, G. D.: Theoretical description of the parabolic approximation/Fourier split-step method of representing electromagnetic propagation in the troposphere, Radio Sci., 26, 381–393, 1991.

Lee, D. S. and Chia, N. K. K.: A particle algorithm for sequential Bayesian parameter estimation and model selection, IEEE Trans. Signal Process., 50, 326–336, 2002.

Park, S. and Fabry, F.: Estimation of near-ground propagation conditions using radar ground echo coverage, J. Atmos. Oceanic Technol., 28, 165–180, 2011.

Richter, J. H.: High resolution tropospheric radar sounding, Radio Sci., 4, 1261–1268, 1969.

Rogers, L. T.: Effects of the variability of atmospheric refractivity on propagation estimates, IEEE Trans. Antennas Propag., 44, 460–465, 1996.

Rogers, L. T., Hattan, C. P., and Stapleton, J. K.: Estimating evaporation duct heights from radar sea echo, Radio Sci., 35, 955–966, 2000.

Sheng, Z.: Tracking refractivity from radar clutter using extended Kalman filter and unscented Kalman filter, available at: http://wulixb.iphy.ac.cn/CN/Y2011/V60/I11/119301 (last access: August 2012), Acta Phys. Sin., 60, 119301, 2011.

Vasudevan, S., Anderson, R. H., Kraut, S., Gerstoft, P., Rogers, L. T., and Krolik, J. L.: Recursive Bayesian electromagnetic refractivity estimation from radar sea clutter, Radio Sci., 42, RS2014, doi:10.1029/2005RS003423, 2007.

Wang, B., Wu, Z. S., Zhao, Z. W., and Wang, H. G.: Retrieving evaporation duct heights from radar sea clutter using particle swarm optimization (PSO) algorithm, Prog. Electromagn. Res. M., 9, 79–91, 2009.

Weckwerth, T. M., Petter, C. R., Fabry, F., Park, S., LeMone, M. A., and Wilson, J. W.: Radar refractivity retrieval: Validation and application to short-term forecasting, J. Appl. Meteorol., 44, 285–300, 2005.

Yan, H. J., Fu, Y., and Hong, Z. J.: Introduction to modern atmospheric refraction, Science and Educational Press, Shanghai, 2006.

Yardim, C., Gerstoft, P., and Hodgkiss, W. S.: Estimation of Radio Refractivity From Radar Clutter Using Bayesian Monte Carlo Analysis, IEEE Trans. Antennas Propag., 54, 1318–1327, 2006.

Yardim, C., Gerstoft, P., and Hodgkiss, W. S.: Statistical maritime radar duct estimation using hybrid genetic algorithm–Markov chain Monte Carlo method, Radio Sci., 42, RS3014, doi:10.1029/2006RS003561, 2007.

Yardim, C., Gerstoft, P., and Hodgkiss, W. S.: Tracking refractivity from clutter using Kalman and particle filters, IEEE Trans. Antennas Propag., 56, 1058–1070, 2008.

Yardim, C., Gerstoft, P., and Hodgkiss, W. S.: Sensitivity analysis and performance estimation of refractivity from clutter techniques, Radio Sci., 44, RS1008, doi:10.1029/2008RS003897, 2009.

Yu, X. L., Xie, Q., and Wang, D. X.: Diurnal cycle of marine atmospheric boundary layer during the 1998 summer monsoon onset over South China Sea, J. Trop. Oceanogr., 28, 31–35, 2009.

Zhao, X. F. and Huang, S. X.: Refractivity from clutter by variational adjoint approach, Prog. Electromagn. Res. B, 33, 153–174, 2011.

Zhao, X. F. and Huang, S. X.: Estimation of atmospheric duct structure using radar sea clutter, J. Atmos. Sci., 69, 2808–2818, 2012.

Zhao, X. F., Huang, S. X., and Du, H. D.: Theoretical analysis and numerical experiments of variational adjoint approach for refractivity estimation, Radio Sci., 46, RS1006, doi:10.1029/2010RS004417, 2011.